Measurement of long-range angular correlations and azimuthal anisotropies in high-multiplicity p+Au collisions at sqrt[s_{NN}]=200 GeV

C. Aidala *et al.* (PHENIX Collaboration)

Phys. Rev. C **95**, 034910 — Published 24 March 2017

DOI: 10.1103/PhysRevC.95.034910

Measurement of long-range angular correlations and azimuthal anisotropies in high-multiplicity p+Au collisions at $\sqrt{s_{_{NN}}} = 200$ GeV

C. Aidala,[39] Y. Akiba,[50,51,*] M. Alfred,[22] V. Andrieux,[39] K. Aoki,[30] N. Apadula,[27] H. Asano,[33,50] C. Ayuso,[39] B. Azmoun,[7] V. Babintsev,[23] N.S. Bandara,[38] K.N. Barish,[8] S. Bathe,[5,51] A. Bazilevsky,[7] M. Beaumier,[8] R. Belmont,[12] A. Berdnikov,[53] Y. Berdnikov,[53] D.S. Blau,[32] M. Boer,[35] J.S. Bok,[44] M.L. Brooks,[35] J. Bryslawskyj,[5,8] V. Bumazhnov,[23] C. Butler,[20] S. Campbell,[13] V. Canoa Roman,[56] R. Cervantes,[56] C.Y. Chi,[13] M. Chiu,[7] I.J. Choi,[24] J.B. Choi,[10,†] Z. Citron,[61] M. Connors,[20,51] N. Cronin,[56] M. Csanád,[16] T. Csörgő,[17,62] T.W. Danley,[45] M.S. Daugherity,[1] G. David,[7] K. DeBlasio,[43] K. Dehmelt,[56] A. Denisov,[23] A. Deshpande,[51,56] E.J. Desmond,[7] A. Dion,[56] D. Dixit,[56] J.H. Do,[63] A. Drees,[56] K.A. Drees,[6] M. Dumancic,[61] J.M. Durham,[35] A. Durum,[23] T. Elder,[17,20] A. Enokizono,[50,52] H. En'yo,[50] S. Esumi,[59] B. Fadem,[40] W. Fan,[56] N. Feege,[56] D.E. Fields,[43] M. Finger,[9] M. Finger, Jr.,[9] S.L. Fokin,[32] J.E. Frantz,[45] A. Franz,[7] A.D. Frawley,[19] Y. Fukuda,[59] C. Gal,[56] P. Gallus,[14] P. Garg,[3,56] H. Ge,[56] F. Giordano,[24] Y. Goto,[50,51] N. Grau,[2] S.V. Greene,[60] M. Grosse Perdekamp,[24] T. Gunji,[11] H. Guragain,[20] T. Hachiya,[50,51] J.S. Haggerty,[7] K.I. Hahn,[18] H. Hamagaki,[11] H.F. Hamilton,[1] S.Y. Han,[18] J. Hanks,[56] S. Hasegawa,[28] T.O.S. Haseler,[20] X. He,[20] T.K. Hemmick,[56] J.C. Hill,[27] K. Hill,[12] R.S. Hollis,[8] K. Homma,[21] B. Hong,[31] T. Hoshino,[21] N. Hotvedt,[27] J. Huang,[7] S. Huang,[60] K. Imai,[28] J. Imrek,[15] M. Inaba,[59] A. Iordanova,[8] D. Isenhower,[1] Y. Ito,[41] D. Ivanishchev,[49] B.V. Jacak,[56] M. Jezghani,[20] Z. Ji,[56] X. Jiang,[35] B.M. Johnson,[7,20] V. Jorjadze,[56] D. Jouan,[47] D.S. Jumper,[24] J.H. Kang,[63] D. Kapukchyan,[8] S. Karthas,[56] D. Kawall,[38] A.V. Kazantsev,[32] V. Khachatryan,[56] A. Khanzadeev,[49] C. Kim,[8,31] D.J. Kim,[29] E.-J. Kim,[10] M. Kim,[31,54] D. Kincses,[16] E. Kistenev,[7] J. Klatsky,[19] P. Kline,[56] T. Koblesky,[12] D. Kotov,[49,53] S. Kudo,[59] K. Kurita,[52] Y. Kwon,[63] J.G. Lajoie,[27] E.O. Lallow,[40] A. Lebedev,[27] S. Lee,[63] M.J. Leitch,[35] Y.H. Leung,[56] N.A. Lewis,[39] X. Li,[35] S.H. Lim,[35,63] L. D. Liu,[48] M.X. Liu,[35] V-R Loggins,[24] V.-R. Loggins,[24] K. Lovasz,[15] D. Lynch,[7] T. Majoros,[15] Y.I. Makdisi,[6] M. Makek,[64] M. Malaev,[49] V.I. Manko,[32] E. Mannel,[7] H. Masuda,[52] M. McCumber,[35] P.L. McGaughey,[35] D. McGlinchey,[12] C. McKinney,[24] M. Mendoza,[8] A.C. Mignerey,[37] D.E. Mihalik,[56] A. Milov,[61] D.K. Mishra,[4] J.T. Mitchell,[7] G. Mitsuka,[51] S. Miyasaka,[50,58] S. Mizuno,[50,59] P. Montuenga,[24] T. Moon,[63] D.P. Morrison,[7] S.I.M. Morrow,[60] T. Murakami,[33,50] J. Murata,[50,52] K. Nagai,[58] K. Nagashima,[21] T. Nagashima,[52] J.L. Nagle,[12] M.I. Nagy,[16] I. Nakagawa,[50,51] H. Nakagomi,[50,59] K. Nakano,[50,58] C. Nattrass,[57] T. Niida,[59] R. Nouicer,[7,51] T. Novák,[17,62] N. Novitzky,[56] R. Novotny,[14] A.S. Nyanin,[32] E. O'Brien,[7] C.A. Ogilvie,[27] J.D. Orjuela Koop,[12] J.D. Osborn,[39] A. Oskarsson,[36] G.J. Ottino,[43] K. Ozawa,[30,59] V. Pantuev,[25] V. Papavassiliou,[44] J.S. Park,[54] S. Park,[50,54,56] S.F. Pate,[44] M. Patel,[27] W. Peng,[60] D.V. Perepelitsa,[7,12] G.D.N. Perera,[44] D.Yu. Peressounko,[32] C.E. PerezLara,[56] J. Perry,[27] R. Petti,[7] M. Phipps,[7,24] C. Pinkenburg,[7] R.P. Pisani,[7] A. Pun,[45] M.L. Purschke,[7] K.F. Read,[46,57] D. Reynolds,[55] V. Riabov,[42,49] Y. Riabov,[49,53] D. Richford,[5] T. Rinn,[27] S.D. Rolnick,[8] M. Rosati,[27] Z. Rowan,[5] J. Runchey,[27] A.S. Safonov,[53] T. Sakaguchi,[7] H. Sako,[28] V. Samsonov,[42,49] M. Sarsour,[20] K. Sato,[59] S. Sato,[28] B. Schaefer,[60] B.K. Schmoll,[57] K. Sedgwick,[8] R. Seidl,[50,51] A. Sen,[27,57] R. Seto,[8] A. Sexton,[37] D. Sharma,[56] I. Shein,[23] T.-A. Shibata,[50,58] K. Shigaki,[21] M. Shimomura,[27,41] T. Shioya,[59] P. Shukla,[4] A. Sickles,[24] C.L. Silva,[35] D. Silvermyr,[36] B.K. Singh,[3] C.P. Singh,[3] V. Singh,[3] M. Slunečka,[9] K.L. Smith,[19] M. Snowball,[35] R.A. Soltz,[34] W.E. Sondheim,[35] S.P. Sorensen,[57] I.V. Sourikova,[7] P.W. Stankus,[46] S.P. Stoll,[7] T. Sugitate,[21] A. Sukhanov,[7] T. Sumita,[50] J. Sun,[56] S. Syed,[20] J. Sziklai,[62] A Takeda,[41] K. Tanida,[28,51,54] M.J. Tannenbaum,[7] S. Tarafdar,[60,61] G. Tarnai,[15] R. Tieulent,[20] A. Timilsina,[27] T. Todoroki,[59] M. Tomášek,[14] C.L. Towell,[1] R.S. Towell,[1] I. Tserruya,[61] Y. Ueda,[21] B. Ujvari,[15] H.W. van Hecke,[35] S. Vazquez-Carson,[12] J. Velkovska,[60] M. Virius,[14] V. Vrba,[14,26] N. Vukman,[64] X.R. Wang,[44,51] Z. Wang,[5] Y. Watanabe,[50,51] Y.S. Watanabe,[11] C.P. Wong,[20] C.L. Woody,[7] C. Xu,[44] Q. Xu,[60] L. Xue,[20] S. Yalcin,[56] Y.L. Yamaguchi,[51,56] H. Yamamoto,[59] A. Yanovich,[23] P. Yin,[12] J.H. Yoo,[31] I. Yoon,[54] H. Yu,[44,48] I.E. Yushmanov,[32] W.A. Zajc,[13] A. Zelenski,[6] S. Zharko,[53] and L. Zou[8]

(PHENIX Collaboration)

[1] *Abilene Christian University, Abilene, Texas 79699, USA*
[2] *Department of Physics, Augustana University, Sioux Falls, South Dakota 57197, USA*
[3] *Department of Physics, Banaras Hindu University, Varanasi 221005, India*
[4] *Bhabha Atomic Research Centre, Bombay 400 085, India*
[5] *Baruch College, City University of New York, New York, New York, 10010 USA*
[6] *Collider-Accelerator Department, Brookhaven National Laboratory, Upton, New York 11973-5000, USA*
[7] *Physics Department, Brookhaven National Laboratory, Upton, New York 11973-5000, USA*
[8] *University of California-Riverside, Riverside, California 92521, USA*
[9] *Charles University, Ovocný trh 5, Praha 1, 116 36, Prague, Czech Republic*
[10] *Chonbuk National University, Jeonju, 561-756, Korea*

[11] *Center for Nuclear Study, Graduate School of Science, University of Tokyo, 7-3-1 Hongo, Bunkyo, Tokyo 113-0033, Japan*
[12] *University of Colorado, Boulder, Colorado 80309, USA*
[13] *Columbia University, New York, New York 10027 and Nevis Laboratories, Irvington, New York 10533, USA*
[14] *Czech Technical University, Zikova 4, 166 36 Prague 6, Czech Republic*
[15] *Debrecen University, H-4010 Debrecen, Egyetem tér 1, Hungary*
[16] *ELTE, Eötvös Loránd University, H-1117 Budapest, Pázmány P. s. 1/A, Hungary*
[17] *Eszterházy Károly University, Károly Róbert Campus, H-3200 Gyñgyös, Mátrai út 36, Hungary*
[18] *Ewha Womans University, Seoul 120-750, Korea*
[19] *Florida State University, Tallahassee, Florida 32306, USA*
[20] *Georgia State University, Atlanta, Georgia 30303, USA*
[21] *Hiroshima University, Kagamiyama, Higashi-Hiroshima 739-8526, Japan*
[22] *Department of Physics and Astronomy, Howard University, Washington, DC 20059, USA*
[23] *IHEP Protvino, State Research Center of Russian Federation, Institute for High Energy Physics, Protvino, 142281, Russia*
[24] *University of Illinois at Urbana-Champaign, Urbana, Illinois 61801, USA*
[25] *Institute for Nuclear Research of the Russian Academy of Sciences, prospekt 60-letiya Oktyabrya 7a, Moscow 117312, Russia*
[26] *Institute of Physics, Academy of Sciences of the Czech Republic, Na Slovance 2, 182 21 Prague 8, Czech Republic*
[27] *Iowa State University, Ames, Iowa 50011, USA*
[28] *Advanced Science Research Center, Japan Atomic Energy Agency, 2-4 Shirakata Shirane, Tokai-mura, Naka-gun, Ibaraki-ken 319-1195, Japan*
[29] *Helsinki Institute of Physics and University of Jyväskylä, P.O.Box 35, FI-40014 Jyväskylä, Finland*
[30] *KEK, High Energy Accelerator Research Organization, Tsukuba, Ibaraki 305-0801, Japan*
[31] *Korea University, Seoul, 136-701, Korea*
[32] *National Research Center "Kurchatov Institute", Moscow, 123098 Russia*
[33] *Kyoto University, Kyoto 606-8502, Japan*
[34] *Lawrence Livermore National Laboratory, Livermore, California 94550, USA*
[35] *Los Alamos National Laboratory, Los Alamos, New Mexico 87545, USA*
[36] *Department of Physics, Lund University, Box 118, SE-221 00 Lund, Sweden*
[37] *University of Maryland, College Park, Maryland 20742, USA*
[38] *Department of Physics, University of Massachusetts, Amherst, Massachusetts 01003-9337, USA*
[39] *Department of Physics, University of Michigan, Ann Arbor, Michigan 48109-1040, USA*
[40] *Muhlenberg College, Allentown, Pennsylvania 18104-5586, USA*
[41] *Nara Women's University, Kita-uoya Nishi-machi Nara 630-8506, Japan*
[42] *National Research Nuclear University, MEPhI, Moscow Engineering Physics Institute, Moscow, 115409, Russia*
[43] *University of New Mexico, Albuquerque, New Mexico 87131, USA*
[44] *New Mexico State University, Las Cruces, New Mexico 88003, USA*
[45] *Department of Physics and Astronomy, Ohio University, Athens, Ohio 45701, USA*
[46] *Oak Ridge National Laboratory, Oak Ridge, Tennessee 37831, USA*
[47] *IPN-Orsay, Univ. Paris-Sud, CNRS/IN2P3, Université Paris-Saclay, BP1, F-91406, Orsay, France*
[48] *Peking University, Beijing 100871, People's Republic of China*
[49] *PNPI, Petersburg Nuclear Physics Institute, Gatchina, Leningrad region, 188300, Russia*
[50] *RIKEN Nishina Center for Accelerator-Based Science, Wako, Saitama 351-0198, Japan*
[51] *RIKEN BNL Research Center, Brookhaven National Laboratory, Upton, New York 11973-5000, USA*
[52] *Physics Department, Rikkyo University, 3-34-1 Nishi-Ikebukuro, Toshima, Tokyo 171-8501, Japan*
[53] *Saint Petersburg State Polytechnic University, St. Petersburg, 195251 Russia*
[54] *Department of Physics and Astronomy, Seoul National University, Seoul 151-742, Korea*
[55] *Chemistry Department, Stony Brook University, SUNY, Stony Brook, New York 11794-3400, USA*
[56] *Department of Physics and Astronomy, Stony Brook University, SUNY, Stony Brook, New York 11794-3800, USA*
[57] *University of Tennessee, Knoxville, Tennessee 37996, USA*
[58] *Department of Physics, Tokyo Institute of Technology, Oh-okayama, Meguro, Tokyo 152-8551, Japan*
[59] *Center for Integrated Research in Fundamental Science and Engineering, University of Tsukuba, Tsukuba, Ibaraki 305, Japan*
[60] *Vanderbilt University, Nashville, Tennessee 37235, USA*
[61] *Weizmann Institute, Rehovot 76100, Israel*
[62] *Institute for Particle and Nuclear Physics, Wigner Research Centre for Physics, Hungarian Academy of Sciences (Wigner RCP, RMKI) H-1525 Budapest 114, POBox 49, Budapest, Hungary*
[63] *Yonsei University, IPAP, Seoul 120-749, Korea*
[64] *University of Zagreb, Faculty of Science, Department of Physics, Bijenička 32, HR-10002 Zagreb, Croatia*

(Dated: February 21, 2017)

We present the first measurements of long-range angular correlations and the transverse momentum dependence of elliptic flow v_2 in high-multiplicity p+Au collisions at $\sqrt{s_{NN}} = 200$ GeV. A comparison of these results with previous measurements in high-multiplicity d+Au and ^{3}He+Au collisions demonstrates a relation between v_2 and the initial collision eccentricity ε_2, suggesting that the observed momentum-space azimuthal anisotropies in these small systems have a collective origin

and reflect the initial geometry. Good agreement is observed between the measured v_2 and hydrodynamic calculations for all systems, and an argument disfavoring theoretical explanations based on initial momentum-space domain correlations is presented. The set of measurements presented here allows us to leverage the distinct intrinsic geometry of each of these systems to distinguish between different theoretical descriptions of the long-range correlations observed in small collision systems.

PACS numbers: 25.75.Dw

* PHENIX Spokesperson: akiba@rcf.rhic.bnl.gov
† Deceased

I. INTRODUCTION

The azimuthal momentum anisotropy of particle emission relative to the participant plane of the collision, as quantified by the Fourier coefficients v_n of the final state particle yield, has long been considered evidence for the formation of a strongly interacting, fluid-like quark-gluon plasma (QGP) in A+A collisions [1]. Viscous hydrodynamics supports a picture in which the initial spatial distribution in energy density, both from intrinsic geometry and fluctuations, is propagated into the final state as anisotropies in momentum space. The success of hydrodynamics in describing various bulk observables of the QGP has lent credence to the notion of hydrodynamic flow as the main driver of the v_n signal in heavy A+A collisions.

However, recent analyses of d+Au and ^{3}He+Au collisions at $\sqrt{s_{_{NN}}} = 200$ GeV [2–5] at the Relativistic Heavy-Ion Collider (RHIC), and p+Pb at $\sqrt{s_{_{NN}}} = 5.02$ TeV, and p+p collisions at $\sqrt{s_{_{NN}}} = 2.76$, 5.02, 7, and 13 TeV [6–12] at the Large Hadron Collider (LHC) have demonstrated the existence of the same kind of azimuthal anisotropy signals commonly interpreted as evidence of collective behavior in larger systems. Notably, a feature known as *the ridge* has been observed, consisting of a near-side (i.e., at small relative azimuth) enhancement in the long-range (i.e., at large relative pseudorapidity) azimuthal two-particle correlation. From these correlations, substantial elliptic (v_2), and triangular (v_3) flow coefficients have been measured in these systems.

Although these observations seem to support the idea of QGP formation in small systems, it is not clear that hydrodynamic expansion would translate initial geometry into final state momentum anisotropy in this regime, where the formed medium is expected to be short-lived. Other explanations have been put forth, including initial state effects from glasma diagrams [13], color recombination [14], and partonic scattering in transport models [15–17]. Transport model calculations, as well as those from hydrodynamics, involve the translation of initial geometry into momentum space via final state interactions. Transport models describe interactions between well defined particles in kinetic theory, while hydrodynamics involves fluid elements. In contrast, glasma diagrams take momentum-space domains as a starting point, resulting in momentum correlations without any final-state interactions. In this initial momentum-space domain picture, the correlations averaged over the event should become weaker in going from p+Au, to d+Au, to ^{3}He+Au as the average is taken over a larger number of domains, thus diluting the strength of the correlation effect. There is no direct correspondence with the initial geometric eccentricity in this picture. A key experimental test to resolve the issue consists in varying the initial geometry of the system to analyze the extent to which it carries into the final state [18].

The PHENIX collaboration has actively pursued this course of study by analyzing data from intrinsically elliptic (d+Au) [2, 3] and triangular (^{3}He+Au) [4] collision systems at $\sqrt{s_{_{NN}}} = 200$ GeV. Viscous hydrodynamics followed by a hadron cascade has been found to accurately reproduce the measured v_n [2, 4, 19–21] for these systems.

This article completes the above suite of studies by presenting two-particle correlations and the transverse momentum (p_T) dependence of v_2 for central p+Au collisions at $\sqrt{s_{_{NN}}} = 200$ GeV. In small system collisions, the term *central* refers to events with high-multiplicity and the correlation with actual impact parameter is weak. These results are compared to those from d+Au and ^{3}He+Au collisions, as well as to available theoretical calculations. We apply the same analysis procedure to all three systems in the same centrality class, to provide a controlled comparison from which to draw conclusions.

II. METHODS

A detailed description of the PHENIX detector can be found in Refs. [22, 23]. For this analysis, charged particles were reconstructed with the two central arm spectrometers, consisting of drift chambers and multi-wire proportional pad chambers (PC), each covering $|\eta| < 0.35$ in pseudorapidity and $\pi/2$ in azimuth. Drift chamber tracks are matched to hits in the third (outermost) layer of the PC, thus limiting the contribution of tracks from decays and photon conversions. The beam-beam counters (BBC) comprise two arrays of 64 quartz radiator Čerenkov detectors, located longitudinally ± 1.44 m away from the center of the interaction region (IR), covering $3.0 < |\eta| < 3.9$ and 2π in azimuth. The forward vertex detector (FVTX) is a silicon detector comprising two identical end-cap assemblies symmetrically located in the longitudinal direction around the IR, covering the pseudorapidity range $1.0 < |\eta| < 3.0$. It uses hit clusters to detect charged particles with an efficiency greater than 95%. The arms of the BBC and FVTX in the Au-going direction (i.e., $\eta < 0$) are designated as the *south* arms and styled BBC-S and FVTX-S, respectively. We use the south arm of each of these two detectors to determine the flow event plane. In addition, the z-vertex of the collision is found using event timing information from both arms of the BBC. In this analysis, a ± 10 cm cut on the collision z-vertex was applied. We compare p+Au correlation functions with those measured in p+p, as described in detail in Ref. [4].

The p+Au data set for this analysis was collected during the 2015 data-taking run at RHIC. It comprises 0.84 billion minimum bias (MB) triggered events and 1.4 billion high-multiplicity (HM) triggered events. The MB trigger

is defined as a coincidence in the same event between the BBC detectors [24] in the Au-going and p-going directions, requiring at least one photomultiplier tube (PMT) firing in each; in this way 84±4% of the total inelastic p+Au cross section is captured. The HM trigger is based on the MB trigger, but imposes the additional requirement of more than 35 photomultiplier tubes firing in the BBC-S. Events that satisfy this trigger condition correspond roughly to the 5% most central event class. The use of this trigger allows us to increase our central event sample size by a factor of 25.

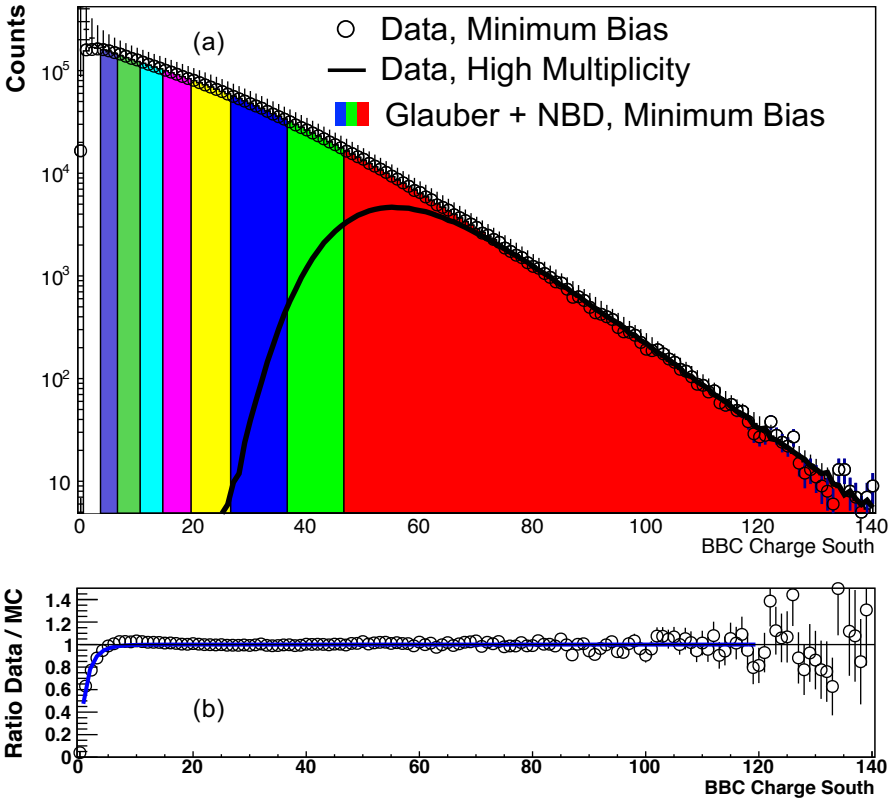

FIG. 1. (a) BBC-S charge measured in real data from MB (open circles) and high multiplicity (solid line) events, where the latter distribution has been scaled down by the respective trigger prescale factor. The Glauber + NBD calculation is shown as [black] crosses. The shaded histogram [colored areas] correspond to the centrality classes for MB events from left to right of 0%–5%, 5%–10%, 10%–20%, 20%–30%, 30%–40%, 40%–50%, 50%–60%, 60%–70%, and 70%–88%. (b) Ratio of real data to the Glauber + NBD calculation for MB events. The blue line is a fit to the trigger efficiency turn-on curve.

In this analysis, we select the 0%–5% most central p+Au events, where centrality classes are defined by the percentiles of the total multiplicity measured in the BBC-S for MB events, following the procedure documented in Ref. [25]. Fig. 1(a) shows the measured distribution of BBC-S charge for the MB and HM trigger event samples, where the latter has been scaled to match the MB distribution. We model the BBC-S charge deposition using a Monte Carlo Glauber model with fluctuations following a negative binomial distribution. The resulting distribution is shown as a histogram, with the colored areas representing various centrality classes. Fig. 1(b) shows the ratio of the measured distribution to the MC Glauber calculation for MB events. The inefficiency observed below 10 units of charge indicates the MB trigger turn-on.

The initial geometry of events in various centrality selections is characterized using a standard Monte Carlo Glauber approach, where nucleon coordinates are smeared by a two-dimensional Gaussian of width $\sigma = 0.4$ fm. In this model, initial state eccentricity ε_2 is computed from initial Gaussian-smeared nucleon coordinates, as shown in Eq. 1.

$$\varepsilon_2 = \frac{\sqrt{\langle r^2 \cos(2\phi)\rangle^2 + \langle r^2 \sin(2\phi)\rangle^2}}{\langle r^2 \rangle} \tag{1}$$

In the above equation, r is the radial nucleon position relative to the centroid of the participants, and ϕ is the nucleon azimuthal angle. The results of this Glauber characterization of the initial geometry are shown in Table I.

TABLE I. Geometric characterization of small system collisions at $\sqrt{s_{NN}}$ = 200 GeV in the 0%–5% centrality class, using Monte Carlo Glauber with nucleon coordinates smeared by a two-dimensional Gaussian of width $\sigma = 0.4$ fm.

	p+Au	d+Au	^{3}He+Au
$\langle N_{\rm coll}\rangle$	9.7 ± 0.6	18.1 ± 1.2	26.1 ± 2.0
$\langle N_{\rm part}\rangle$	10.7 ± 0.6	17.8 ± 1.2	25.1 ± 1.6
Glauber $\langle \varepsilon_2 \rangle$	0.23 ± 0.01	0.54 ± 0.04	0.50 ± 0.02

The quantities characterizing the event geometry are the same within uncertainties for both the MB and HM event samples.

III. RESULTS

Long-range angular correlations are constructed between charged tracks in the PHENIX central arms at a given p_T, and charge deposited in the BBC-S PMTs, for central p+Au collisions. The distribution of these track-PMT pairs is constructed over relative azimuth as given in Eq. 2, with the normalized correlation function given by Eq. 3, following Ref. [26]:

$$S(\Delta\phi, p_T) = \frac{d(w_{\rm PMT} N^{{\rm track}(p_T)-{\rm PMT}}_{\rm Same\ event})}{d\Delta\phi}, \tag{2}$$

$$C(\Delta\phi, p_T) = \frac{S(\Delta\phi, p_T)}{M(\Delta\phi, p_T)} \frac{\int_0^{2\pi} M(\Delta\phi, p_T)\, d\Delta\phi}{\int_0^{2\pi} S(\Delta\phi, p_T)\, d\Delta\phi}. \tag{3}$$

The weights $w_{\rm PMT}$ for each pair correspond to the charge in the PMTs comprised in that particular pair. The signal distribution S is constructed from pairs in the same event. The mixed distribution M is constructed using pairs from different events in the same centrality class and collision vertex bin. Ten equally sized bins are used within the range of $|z| < 10$ cm in the event mixing.

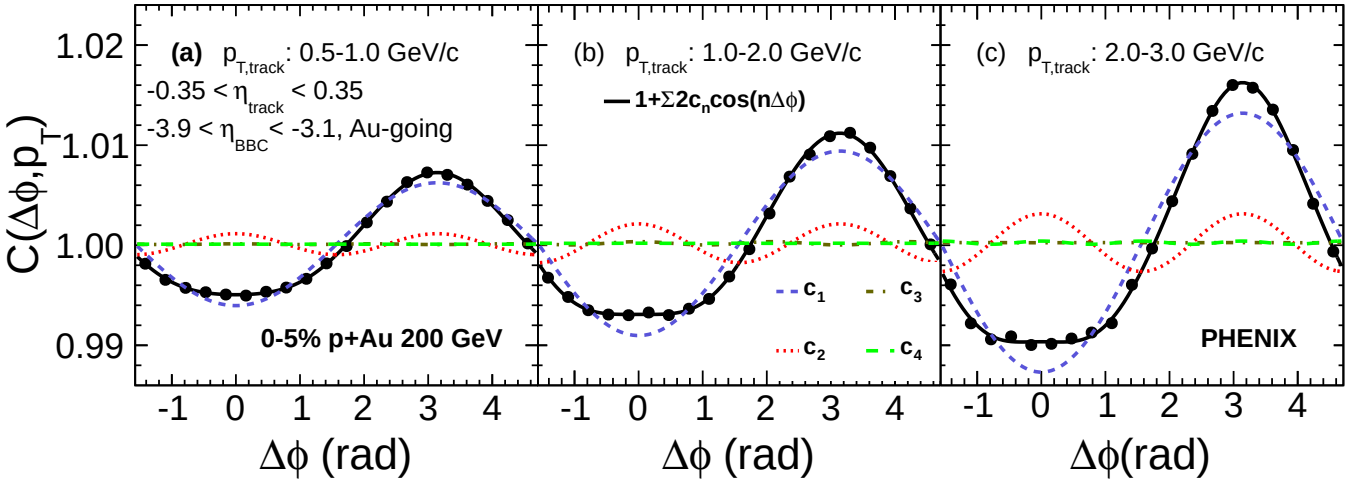

FIG. 2. Long-range angular correlations $C(\Delta\phi, p_T)$ constructed with central arm tracks and BBC-S PMT pairs, in 0%–5% central p+Au collisions at $\sqrt{s_{NN}}$ = 200 GeV. From left to right, correlations are shown for various track p_T categories: (a) 0.5–1.0 GeV/c, (b) 1.0–2.0 GeV/c, and (c) 2.0–3.0 GeV/c. We fit each correlation with a four-term cosine Fourier series. The harmonic c_1 is shown as a short-dashed line; c_2, as a dotted line; c_3, as a dash-dot line; c_4, as a long-dashed line. The total fit is shown as a solid line.

The resulting correlation functions for three track p_T selections are shown in Fig. 2. Each one is fit with a four-term cosine Fourier series, $C(\Delta\phi) = \sum_{n=1}^{4} 2c_n \cos(n\Delta\phi)$. The magnitude of the second harmonic c_2 as a function of p_T is shown with red circles in Fig. 3 panel (a). The contribution of elementary processes (e.g., jet fragmentation,

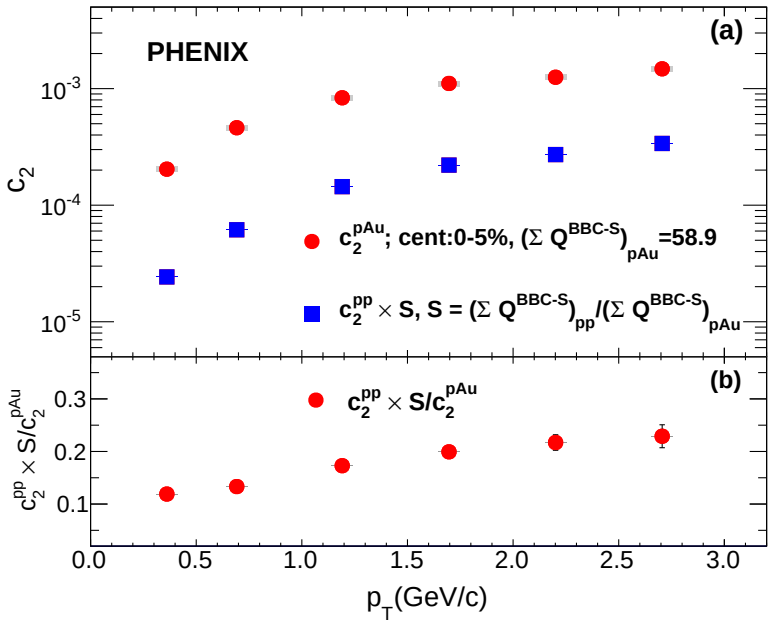

FIG. 3. (a) The second order harmonic coefficients $c_2(p_T)$ for long range angular correlations in 0%–5% p+Au collisions, as well as for MB p+p collisions. The latter are scaled down by the factor $\left(\sum Q^{\mathrm{BBC-S}}\right)_{p+p} / \left(\sum Q^{\mathrm{BBC-S}}\right)_{p\mathrm{Au}}$. (b) The ratio of the two harmonics is plotted with the corresponding statistical errors.

resonance decays, and momentum conservation effects) to the measured c_2 in p+Au can be estimated quantitatively using previously published c_2 data from p+p at the same collision energy [4], scaled down by an appropriate factor to account for the higher multiplicity in p+Au. We choose the scale factor to be the ratio of the total charge deposited in the BBC-S (i.e., $Q^{\mathrm{BBC-S}}$) in p+p relative to p+Au, as shown in Eq. 4, because we can think of a p+Au event as the superposition of N independent nucleon-nucleon collisions, where the correlation strength from a single collision scales inversely with N.

$$c_2^{p\mathrm{Au\ elementary}}(p_T) \simeq c_2^{p+p}(p_T) \frac{\left(\sum Q^{\mathrm{BBC-S}}\right)_{p+p}}{\left(\sum Q^{\mathrm{BBC-S}}\right)_{p\mathrm{Au}}}. \tag{4}$$

The scaled down reference c_2 is shown as blue squares in Fig. 3, panel (a). The ratio of c_2 in the scaled-down p+p reference to p+Au is shown in panel (b). From this ratio, it can be seen that the relative correlation strength in p+Au from elementary processes is at most 23% at the highest p_T. Because this procedure constitutes an approximation to quantify the nonflow correlation strength, which may be affected by other factors not considered in this analysis, we do not subtract it from the total signal, treating it instead as a source of systematic uncertainty. Even though the p+Au and the p+p baseline data were collected in different years, where potential changes in detector performance could affect our results, we verified that using p+p data from various run periods has an effect of at most 3% on the calculated nonflow contribution.

It is noteworthy that, unlike in d+Au [20] and ^{3}He+Au [26] collisions at the same centrality, the long-range angular correlations in p+Au do not exhibit a discernible near-side peak, yet possess a nonnegligible second harmonic component. The nonflow contribution from elementary processes and momentum conservation becomes more dominant as the system size and particle multiplicity decrease. This results in a larger $|c_1|$ and thus a smaller $|c_2/c_1|$ ratio, and hence in a less discernible near-side peak in p+Au.

Having quantified the strength of the correlations from elementary processes, we determine the second Fourier coefficient v_2 of the single-particle azimuthal distributions, which is typically associated with collective elliptic flow, using the event plane method as described in Ref. [27]. Namely, we measure

$$v_2(p_T) = \frac{\langle \cos 2(\phi_{\mathrm{Particle}}(p_T) - \Psi_2^{\mathrm{FVTX-S}}) \rangle}{\mathrm{Res}(\Psi_2^{\mathrm{FVTX-S}})} \tag{5}$$

for charged hadrons at midrapidity, where the second order event plane $\Psi_2^{\rm FVTX-S}$ is determined for every event using the FVTX-S detector. Its resolution $\mathrm{Res}(\Psi_2)$ is computed using the standard three-subevent method [27], correlating measurements in the BBC-S, FVTX-S, and the central arms. This results in $\mathrm{Res}(\Psi_2^{\rm FVTX-S}) = 0.171$. It is also possible to measure the event plane using the BBC-S. In that case, we obtain a lower resolution $\mathrm{Res}(\Psi_2^{\rm BBC-S}) = 0.062$, and v_2 values that differ from the FVTX-S measurement by approximately 3%. The very good agreement of v_2 measured using the BBC-S and FVTX-S event planes is interesting, because the pseudorapidity gaps relative to the midrapidity tracks are $|\Delta\eta| > 2.65$ and $|\Delta\eta| > 0.65$, respectively.

The main sources of systematic uncertainty in the $v_2(p_T)$ measurement are: (1) track background from photon conversion and weak decays, whose magnitude we determine at 2% relative to the measured v_2 by varying the spatial matching windows in the PC3 from 3σ to 2σ; (2) Multiple collisions per bunch crossing (i.e., event pile-up) that are observed to occur at an average rate of 8% in the 0%–5% central p+Au collisions. Low luminosity and high-luminosity subsets of the data were analyzed separately and the systematic uncertainty in the $v_2(p_T)$ value is determined to be asymmetric $^{+4\%}_{-0\%}$, because the v_2 values were found to decrease in the events that contain a larger fraction of pile-up; (3) Non-flow correlations from elementary processes that enhance the v_2 values, whose contribution we estimate from Fig. 3, assigning a p_T-dependent asymmetric uncertainty with a maximum value of $^{+0}_{-23}$% for the highest p_T bin. This can be compared to the corresponding $^{+0}_{-9}$% [3] and $^{+0}_{-7}$% [4] systematic uncertainties in d+Au and ^{3}He+Au collisions, respectively; (4) The asymmetry between the east ($\pi/2 < \phi < 3\pi/2$) and west ($-\pi/2 < \phi < \pi/2$) acceptance of the detectors due to an offset of 3.6 mrad between the colliding beams and the longitudinal axis of PHENIX, necessary for running p+Au at the same momentum per nucleon. We applied a corresponding counter-rotation to every central arm track and detector element in the FVTX and BBC, which were also reweighted to restore their uniformity in azimuth. We assign a value of 5% for this systematic uncertainty by taking the difference of v_2 as measured independently in the east and the west arms after applying the above corrections; (5) The difference in the $v_2(p_T)$ values when measured independently using the BBC-S and FVTX event planes, which we observe to differ by ±3%.

TABLE II. Systematic uncertainties given as a percent of the v_2 measurement. Note that the nonflow contribution is p_T dependent and the value here quoted corresponds to the highest measured p_T.

Source	Systematic Uncertainty	Type
Track Background	2.0%	A
Event Pile-up	$^{+4}_{-0}$%	B
Non-Flow	$^{+0}_{-23}$%	B
Beam Angle	5.0%	C
Event-Plane Detectors	3%	C

Table II summarizes of all these systematic uncertainties, categorized by type:

(A) point-to-point uncorrelated between p_T bins,

(B) point-to-point correlated between p_T bins,

(C) overall normalization uncertainty in which all points are scaled by the same multiplicative factor.

The resulting v_2 measurement for p+Au, compared to d+Au [3] and ^{3}He+Au [4] in the same 0%–5% centrality class, is shown in Fig. 4. The d+Au data, as presented in Ref. [3], did not include nonflow contributions in its systematic uncertainties, which are now accounted for in the systematics shown in Fig. 4. In all cases, there is a substantial v_2 that rises with p_T. It is notable that the v_2 values for d+Au and ^{3}He+Au are consistent within uncertainties, as are their eccentricities ε_2 listed in Table I. The p+Au collisions have a significantly lower v_2 and a correspondingly lower calculated ε_2. At the same time, the ordering of v_2 from p+Au, to d+Au, to ^{3}He+Au also follows the expected increasing order of particle multiplicity. In the case of d+Au and ^{3}He+Au, for the 0%–5% most central events, the published values for midrapidity charged particle density are $dN_{ch}/d\eta = 20.8 \pm 1.5$ and 26.3 ± 1.8, respectively [28]. This quantity has not yet been measured in p+Au collisions.

IV. DISCUSSION

Also shown in Fig. 4 are v_2 calculations for each system from the SONIC hydrodynamic model [29], which incorporates standard Monte Carlo Glauber initial conditions followed by viscous hydrodynamics with $\eta/s = 0.08$, and a transition to a hadronic cascade at $T = 170$ MeV. It is notable that these calculations for each system are matched to the charged particle density at midrapidity, with the exact values for 0%–5% centrality of 10.0, 20.0, and 27.0, for p+Au, d+Au, and ^{3}He+Au collisions, respectively [29]. Again, note that $dN_{ch}/d\eta$ has not been measured for p+Au, and that the value of 10.0 was extrapolated from measurements in the other two systems [29]. We thus see

that the calculation includes both the geometry-related change in eccentricity and the relative collision multiplicity. In all cases, a good agreement is seen within uncertainties between the data and the calculation. These observations strongly support the notion of initial geometry, coupled to the hydrodynamic evolution of the medium as a valid framework to understand small system collectivity.

To further explore this idea, we divide the v_2 curves by their corresponding ε_2 from Table I, attempting to establish a scaling relation between the two quantities. Fig. 5 shows that the ratios do not collapse to a common value. As expected, this behavior is also reproduced by the SONIC calculation, because both data and calculation are divided by the same ε_2 values. The lack of scaling in the SONIC calculation can be understood from d+Au events where the neutron and proton from the deuteron projectile are far separated and create two hot spots upon impacting the Au nucleus. These events have a large ε_2, but can result in small v_2 if the two hot spots evolve separately, never combining within the hydrodynamic time evolution. This effect is present in the d+Au and ^{3}He+Au systems, and lowers the average v_2/ε_2 as detailed in Ref. [18].

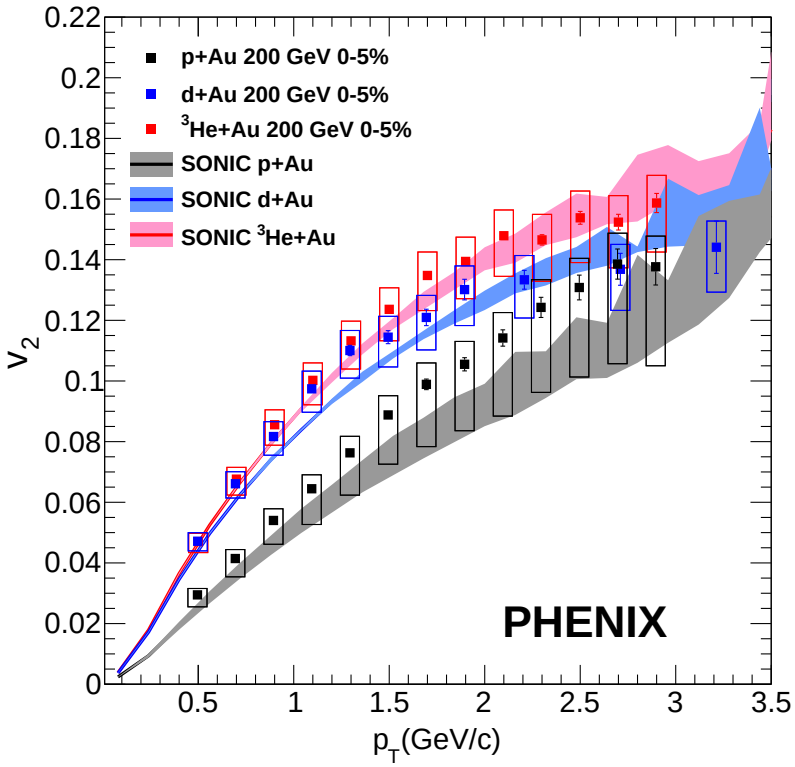

FIG. 4. v_2 of charged hadrons within $|\eta| < 0.35$ in 0%–5% (bottom [gray] curve) p+Au, (middle [blue] curve) d+Au, and (top [red] curve) ^{3}He+Au central collisions, compared to hydrodynamic calculations using the SONIC model, matched to the same multiplicity as the data. Note that the data points shown include nonflow contributions, whose estimated magnitude is accounted for in the asymmetric systematic uncertainties.

Figure 6 shows $v_2(p_T)$ for 0%–5% central p+Au, d+Au, and ^{3}He+Au events, along with theoretical predictions available in the literature, most notably from hydrodynamics with Glauber initial conditions (SONIC [29] and SUPERSONIC [19]), hydrodynamics with IP-Glasma initial conditions [30], and A-Multi-Phase-Transport Model (AMPT) [31].

The SUPERSONIC model uses the same prescription for initial conditions, hydrodynamic expansion, and hadronic cascade as SONIC, yet additionally incorporates pre-equilibrium dynamics with a calculation in the framework of the AdS/CFT correspondence [32–34]. These two models agree well with the data within uncertainties, supporting the idea of initial geometry as the driver of the v_n signal. Furthermore, this illustrates how these results impose useful constraints to reduce the number of *free parameters* of the model, because many such parameters must be identical across systems, e.g., η/s, the transition temperature to a hadron cascade, and the Monte Carlo Glauber smearing of nucleon coordinates of $\sigma = 0.4$ fm.

Calculations using IP-Glasma initial conditions followed by viscous hydrodynamics have been successfully used to describe collectivity in A+A collisions [35]. It is notable that in these calculations the glasma framework is used only to determine the initial spatial configuration as input to hydrodynamics; there is no glasma diagram or momentum-domain physics incorporated, such that all of the collectivity arises from final-state interactions. When this framework

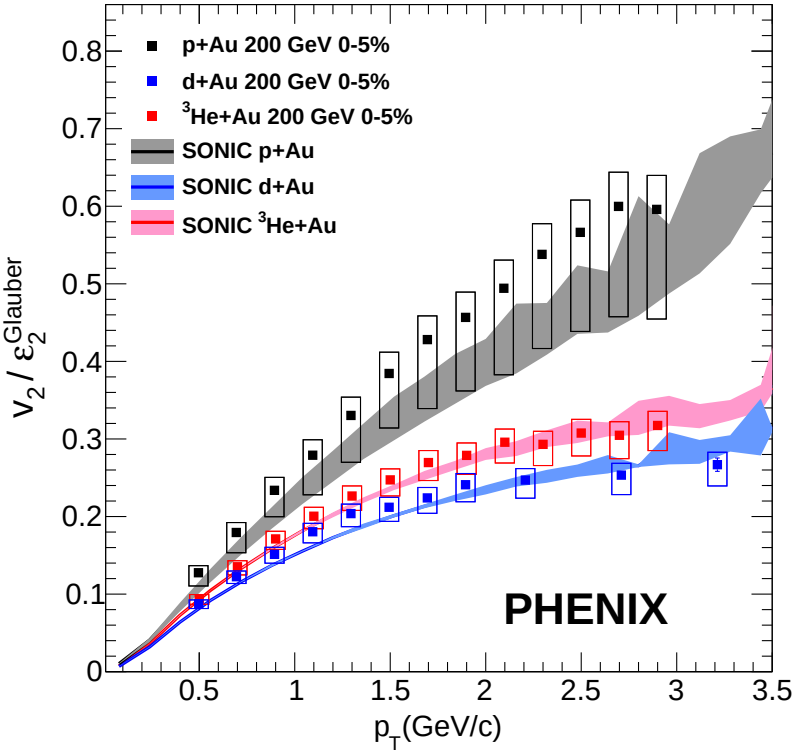

FIG. 5. v_2 of charged hadrons within $|\eta| < 0.35$ in 0%–5% (top [gray] curve) p+Au, (center [red] curve) d+Au and (bottom [blue] curve) ^{3}He+Au central collisions, divided by their corresponding eccentricity ε_2 from Glauber calculations, compared to SONIC calculations of the same quantity. Note that the data points shown include nonflow contributions, whose estimated magnitude is accounted for in the asymmetric systematic uncertainties.

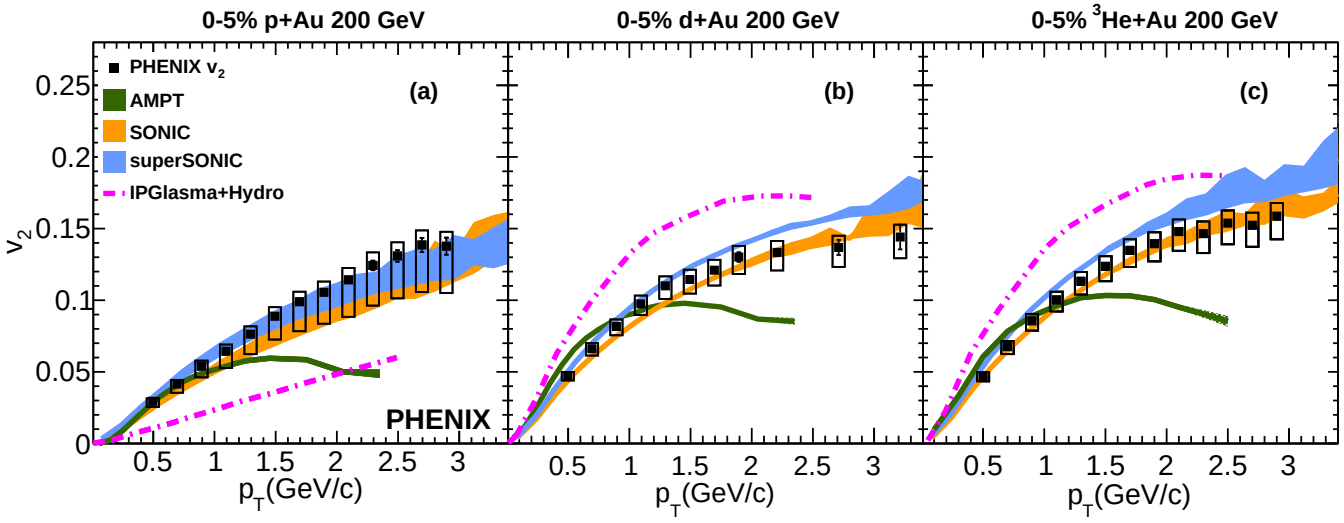

FIG. 6. Transverse momentum dependence of v_2 in central 0%–5% (a) p+Au, (b) d+Au, and (c) ^{3}He+Au collisions at $\sqrt{s_{NN}} = 200$ GeV. Theoretical calculations from (solid [gray] curve) AMPT, (central [orange] band) SONIC, (top [blue] band) SUPERSONIC, and (dot-dashed [magenta] curves) IPGlasma+Hydro are shown in each panel. Note that the data points shown include nonflow contributions, whose estimated magnitude is accounted for in the asymmetric systematic uncertainties.

is applied to small collision systems with $\eta/s = 0.12$ and $b < 2$ fm, as shown in Fig. 6, the calculation substantially overestimates the data for d+Au and ^{3}He+Au, while underestimating it for p+Au. This follows from the fact that IP-Glasma generates very *circular* initial conditions for p+Au, corresponding to very low ε_2 values; however, the presence of several hot spots in d+Au and ^{3}He+Au result in IP-Glasma values for ε_2 more comparable to those from Glauber. This is shown in Table III.

TABLE III. Initial eccentricity ε_2 of small systems at $\sqrt{s_{NN}} = 200$ GeV for 0%–5% centrality from Monte Carlo Glauber initial conditions smeared with a two-dimensional Gaussian of width $\sigma = 0.4$ fm, and IP-Glasma initial conditions.

	p+Au	d+Au	^{3}He+Au
Glauber $\langle\varepsilon_2\rangle$	0.23 ± 0.01	0.54 ± 0.04	0.50 ± 0.02
IP-Glasma $\langle\varepsilon_2\rangle$	0.10 ± 0.02	0.59 ± 0.01	0.55 ± 0.01

In the case of d+Au and ^{3}He+Au, a better agreement with data can be achieved by increasing the value of η/s or by including a hadronic cascade stage. However, doing so would lower the prediction for p+Au even further. This demonstrates that IP-Glasma does not generate the appropriate initial conditions to account for measured v_n via hydrodynamic flow.

It is important to notice that additional degrees of freedom for the geometry of p+Au collisions arise from fluctuations of the shape of the proton, as described in Ref. [36]. The contribution of this effect to the measured elliptic flow may be constrained by p+p data, and also possibly by varying the target in other p+A systems.

An additional framework accounting for subnucleonic degrees of freedom extends the Monte Carlo Glauber approach to also incorporate collisions between constituent quarks [37]. Recently, this framework has been successfully applied to the description of midrapidity charged particle multiplicity and transverse energy production [28, 38]. Different implementations of constituent quark Monte Carlo Glauber calculations are detailed in Refs. [39–42]. In Fig. 13(f) of Ref. [39], the initial eccentricities ε_2 in p+Au, d+Au, and ^{3}He+Au obtained by incorporating constituent quarks in addition to multiplicity fluctuations are found to be $\varepsilon_2 = 0.42$, 0.54, and 0.54, respectively. This calculation assumes a Gaussian density distribution of low-x gluons around each constituent quark, of width $\sigma_g = 0.3$ fm. It is interesting to note that the d+Au and ^{3}He+Au systems show little sensitivity to the incorporation of both constituent quarks and multiplicity fluctuations into the calculation of the initial ε_2. Conversely, under the same circumstances, p+Au has a substantially larger ε_2 than in the models shown in Table III. Ref. [39] also presents calculations incorporating nucleonic degrees of freedom and multiplicity fluctuations, in which case a lower $\varepsilon_2 = 0.34$ is obtained for p+Au. This shows that, when compared to the Glauber ε_2 for p+Au in Table III, quark-level degrees of freedom and multiplicity fluctuations may both play a significant role. Hydrodynamic calculations with these initial conditions will be of interest for future studies.

Finally, AMPT combines partonic and hadronic scattering in a single model. Central AMPT events with impact parameter $b < 2$ have a midrapidity $dN_{ch}/d\eta = 8.1$, 14.8, and 20.7 for p+Au, d+Au, and ^{3}He+Au, respectively. These were generated with the same Monte Carlo Glauber initial conditions used to characterize event geometry, and thus have very similar eccentricities to those given in Table I. Using the initial Glauber geometry information to compute v_2 relative to the participant plane [17] yields results that agree reasonably well with the data below $p_T \approx 1$ GeV/c, yet underpredict them at higher p_T. It is noteworthy that despite the very different physics of AMPT compared to the other models, it has successfully been applied to a variety of systems at RHIC and the LHC. See, for example, Refs. [16, 17, 43, 44]

V. SUMMARY

We have presented results on azimuthal anisotropy and elliptic flow in central p+Au at $\sqrt{s_{NN}} = 200$ GeV, compared with v_2 in d+Au and ^{3}He+Au collisions. These results impose strong constraints on any model attempting to describe small system collectivity, whether by the formation of strongly interacting hot nuclear matter, or other mechanisms. We observe an imperfect scaling of v_2 with ε_2, well reproduced by hydrodynamics, providing strong evidence for initial geometry as the source of final-state momentum anisotropy in these systems. This disfavors other explanations based on initial-state momentum space domain effects. Further insight into the nature of small system collectivity can be gained by analyzing the centrality and collision energy dependence of v_2, and will be the subject of future studies.

ACKNOWLEDGMENTS

We thank the staff of the Collider-Accelerator and Physics Departments at Brookhaven National Laboratory and the staff of the other PHENIX participating institutions for their vital contributions. We acknowledge support from the Office of Nuclear Physics in the Office of Science of the Department of Energy, the National Science Foundation, Abilene Christian University Research Council, Research Foundation of SUNY, and Dean of the College of Arts and Sciences, Vanderbilt University (U.S.A), Ministry of Education, Culture, Sports, Science, and Technology and the Japan Society for the Promotion of Science (Japan), Conselho Nacional de Desenvolvimento Científico e Tecnológico and Fundação de Amparo à Pesquisa do Estado de São Paulo (Brazil), Natural Science Foundation of China (People's Republic of China), Croatian Science Foundation and Ministry of Science, Education, and Sports (Croatia), Ministry of Education, Youth and Sports (Czech Republic), Centre National de la Recherche Scientifique, Commissariat à l'Énergie Atomique, and Institut National de Physique Nucléaire et de Physique des Particules (France), Bundesministerium für Bildung und Forschung, Deutscher Akademischer Austausch Dienst, and Alexander von Humboldt Stiftung (Germany), National Science Fund, OTKA, Károly Róbert University College, and the Ch. Simonyi Fund (Hungary), Department of Atomic Energy and Department of Science and Technology (India), Israel Science Foundation (Israel), Basic Science Research Program through NRF of the Ministry of Education (Korea), Physics Department, Lahore University of Management Sciences (Pakistan), Ministry of Education and Science, Russian Academy of Sciences, Federal Agency of Atomic Energy (Russia), VR and Wallenberg Foundation (Sweden), the U.S. Civilian Research and Development Foundation for the Independent States of the Former Soviet Union, the Hungarian American Enterprise Scholarship Fund, and the US-Israel Binational Science Foundation.

[1] U. Heinz and R. Snellings, "Collective flow and viscosity in relativistic heavy-ion collisions," Ann. Rev. Nucl. Part. Sci. **63**, 123 (2013).
[2] A. Adare *et al.* (PHENIX Collaboration), "Quadrupole Anisotropy in Dihadron Azimuthal Correlations in Central d+Au Collisions at $\sqrt{s_{NN}} = 200$ GeV," Phys. Rev. Lett. **111**, 212301 (2013).
[3] A. Adare *et al.* (PHENIX Collaboration), "Measurement of long-range angular correlation and quadrupole anisotropy of pions and (anti)protons in central d+Au collisions at $\sqrt{s_{NN}}$=200 GeV," Phys. Rev. Lett. **114**, 192301 (2015).
[4] A. Adare *et al.* (PHENIX Collaboration), "Measurements of elliptic and triangular flow in high-multiplicity ^{3}He+Au collisions at $\sqrt{s_{NN}} = 200$ GeV," Phys. Rev. Lett. **115**, 142301 (2015).
[5] L. Adamczyk *et al.* (STAR Collaboration), "Effect of event selection on jetlike correlation measurement in d+Au collisions at $\sqrt{s_{NN}} = 200$ GeV," Phys. Lett. B **743**, 333 (2015).
[6] B. Abelev *et al.* (ALICE Collaboration), "Long-range angular correlations on the near and away side in p-Pb collisions at $\sqrt{s_{NN}} = 5.02$ TeV," Phys. Lett. B **719**, 29 (2013).
[7] G. Aad *et al.* (ATLAS Collaboration), "Observation of Associated Near-Side and Away-Side Long-Range Correlations in $\sqrt{s_{NN}} = 5.02$ TeV Proton-Lead Collisions with the ATLAS Detector," Phys. Rev. Lett. **110**, 182302 (2013).
[8] S. Chatrchyan *et al.* (CMS Collaboration), "Observation of long-range, near-side angular correlations in pPb collisions at the LHC," Phys. Lett. B **718**, 795 (2013).
[9] V. Khachatryan *et al.* (CMS Collaboration), "Measurement of long-range near-side two-particle angular correlations in *pp* collisions at $\sqrt{s} = 13$ TeV," Phys. Rev. Lett. **116**, 172302 (2016).
[10] G. Aad *et al.* (ATLAS Collaboration), "Observation of Long-Range Elliptic Azimuthal Anisotropies in $\sqrt{s}$ =13 and 2.76 TeV *pp* Collisions with the ATLAS Detector," Phys. Rev. Lett. **116**, 172301 (2016).
[11] V. Khachatryan *et al.* (CMS Collaboration xyz), "Observation of Long-Range Near-Side Angular Correlations in Proton-Proton Collisions at the LHC," (), J. High Energy Phys. **09 (2010)** 091.
[12] V. Khachatryan *et al.* (CMS Collaboration xyz), "Evidence for collectivity in *pp* collisions at the LHC," (), arXiv:1606.06198.
[13] K. Dusling and R. Venugopalan, "Azimuthal Collimation of Long Range Rapidity Correlations by Strong Color Fields in High Multiplicity Hadron-Hadron Collisions," Phys. Rev. Lett. **108**, 262001 (2012).
[14] A. Ortiz Velasquez, P. Christiansen, E. Cuautle Flores, I.A. Maldonado Cervantes, and G. Paic, "Color Reconnection and Flowlike Patterns in *pp* Collisions," Phys. Rev. Lett. **111**, 042001 (2013).
[15] A. Bzdak and G.-L. Ma, "Elliptic and Triangular Flow in p-Pb and Peripheral Pb-Pb Collisions from Parton Scatterings," Phys. Rev. Lett. **113**, 252301 (2014).
[16] G.-L. Ma and A. Bzdak, "Long-range azimuthal correlations in proton-proton and proton-nucleus collisions from the incoherent scattering of partons," Phys. Lett. B **739**, 209 (2014).
[17] J. D. Orjuela Koop, A. Adare, D. McGlinchey, and J. L. Nagle, "Azimuthal anisotropy relative to the participant plane from a multiphase transport model in central p+Au, d+Au , and ^{3}He+Au collisions at $\sqrt{s_{NN}} = 200$ GeV," Phys. Rev. C **92**, 054903 (2015).
[18] J. L. Nagle, A. Adare, S. Beckman, T. Koblesky, J. O. Koop, D. McGlinchey, P. Romatschke, J. Carlson, J. E. Lynn, and M. McCumber, ""Exploiting intrinsic triangular geometry in relativistic ^{3}he+au collisions to disentangle medium

properties",," Phys. Rev. Lett. **113**, 112301 (2014).
[19] P. Romatschke, "Light-Heavy Ion Collisions: A window into pre-equilibrium QCD dynamics?" Eur. Phys. J. C **75**, 305 (2015).
[20] A. Adare *et al.* (PHENIX Collaboration), "Measurement of long-range angular correlation and quadrupole anisotropy of pions and (anti)protons in central d+Au collisions at $\sqrt{s_{NN}}$=200 GeV," Phys. Rev. Lett. **114**, 192301 (2015).
[21] P. Bozek and W. Broniowski, "Hydrodynamic modeling of ^{3}He-Au collisions at $\sqrt{s_{NN}}$=200 GeV," Phys. Lett. B **747**, 135 (2015).
[22] K. Adcox *et al.* (PHENIX Collaboration), "PHENIX detector overview," Nucl. Instrum. Methods Phys. Res., Sec. A **499**, 469 (2003).
[23] C. Aidala *et al.*, "The PHENIX Forward Silicon Vertex Detector," Nucl. Instrum. Methods Phys. Res., Sec. A **755**, 44 (2014).
[24] M. et al. Allen, "{PHENIX} inner detectors," Nucl. Instrum. Methods Phys. Res., Sec. A **499**, 549 (2003), The Relativistic Heavy Ion Collider Project: RHIC and its Detectors.
[25] A. Adare *et al.* (PHENIX Collaboration), "Centrality categorization for $R_{p(d)+Au}$ in high-energy collisions," Phys. Rev. C **90**, 034902 (2014).
[26] A. Adare *et al.* (PHENIX Collaboration), "Measurements of Elliptic and Triangular Flow in High-Multiplicity ^{3}He+Au Collisions at $\sqrt{s_{NN}} = 200$ GeV," Phys. Rev. Lett. **115**, 142301 (2015).
[27] A. M. Poskanzer and S. A. Voloshin, "Methods for analyzing anisotropic flow in relativistic nuclear collisions," Phys. Rev. C **58**, 1671 (1998).
[28] A. Adare *et al.* (PHENIX Collaboration), "Transverse energy production and charged-particle multiplicity at midrapidity in various systems from $\sqrt{s_{NN}} = 7.7$ to 200 GeV," Phys. Rev. C **93**, 024901 (2016).
[29] M. Habich, J. L. Nagle, and P. Romatschke, "Particle spectra and HBT radii for simulated central nuclear collisions of C+C, Al+Al, Cu+Cu, Au+Au, and Pb+Pb from $\sqrt{s} = 62.4$–2760 GeV," Eur. Phys. J. C **75**, 15 (2015).
[30] B. Schenke and R. Venugopalan, "Collective effects in light-heavy ion collisions," *Proceedings, 24th International Conference on Ultra-Relativistic Nucleus-Nucleus Collisions (Quark Matter 2014)*, Nucl. Phys. A **931**, 1039 (2014).
[31] Z.-W. Lin, C. M. Ko, B.-A. Li, B. Zhang, and S. Pal, "Multiphase transport model for relativistic heavy ion collisions," Phys. Rev. C **72**, 064901 (2005).
[32] W. van der Schee, P. Romatschke, and S. Pratt, "Fully Dynamical Simulation of Central Nuclear Collisions," Phys. Rev. Lett. **111**, 222302 (2013).
[33] P. M. Chesler and L. G. Yaffe, "Holography and off-center collisions of localized shock waves," J. High Energy Phys. **10 (2015)** 070.
[34] P. Romatschke and J. D. Hogg, "Pre-Equilibrium Radial Flow from Central Shock-Wave Collisions in AdS5," J. High Energy Phys. **04 (2013)** 048.
[35] C. Gale, S. Jeon, B. Schenke, P. Tribedy, and R. Venugopalan, "Event-by-event anisotropic flow in heavy-ion collisions from combined Yang-Mills and viscous fluid dynamics," Phys. Rev. Lett. **110**, 012302 (2013).
[36] S. Schlichting and B. Schenke, "The shape of the proton at high energies," Phys. Lett. B **739**, 313 (2014).
[37] S. Eremin and S. Voloshin, "Nucleon participants or quark participants?" Phys. Rev. C **67**, 064905 (2003).
[38] S. S. Adler *et al.* (PHENIX Collaboration), "Transverse-energy distributions at midrapidity in p+p , d+Au , and Au+Au collisions at $\sqrt{s_{NN}} = 62.4$–200 GeV and implications for particle-production models," Phys. Rev. C **89**, 044905 (2014).
[39] K. Welsh, J. Singer, and U. W. Heinz, "Initial state fluctuations in collisions between light and heavy ions," Phys. Rev. C **94**, 024919 (2016).
[40] C. Loizides, "Glauber modeling of high-energy nuclear collisions at sub-nucleon level," Phys. Rev. C **94**, 024914 (2016).
[41] P. Bozek, W. Broniowski, and M. Rybczynski, "Wounded quarks in $A + A$, $p + A$, and $p + p$ collisions," Phys. Rev. C **94**, 014902 (2016).
[42] J. T. Mitchell, D. V. Perepelitsa, M. J. Tannenbaum, and P. W. Stankus, "Tests of constituent-quark generation methods which maintain both the nucleon center of mass and the desired radial distribution in Monte Carlo Glauber models," Phys. Rev. C **93**, 054910 (2016).
[43] A. Adare *et al.* (PHENIX Collaboration), "Measurements of directed, elliptic, and triangular flow in Cu+Au collisions at $\sqrt{s_{NN}} = 200$ GeV," arXiv:1509.07784.
[44] G.-L. Ma and Z.-W. Lin, "Predictions for $\sqrt{s_{NN}} = 5.02$ TeV Pb+Pb Collisions from a Multi-Phase Transport Model," Phys. Rev. C **93**, 054911 (2016).